Engineering a cytochrome P450 for demethylation of lignin-derived aromatic aldehydes

Emerald S. Ellis,[a‡] Daniel J. Hinchen,[b‡] Alissa Bleem,[c,d‡] Lintao Bu,[c] Sam J.B. Mallinson,[b†] Mark D. Allen,[b] Bennett R. Streit,[a] Melodie M. Machovina,[a¶] Quinlan V. Doolin,[a] William E. Michener,[c] Christopher W. Johnson,[c] Brandon C. Knott,[c] Gregg T. Beckham,[c,d]* John E. McGeehan,[b]* Jennifer L. DuBois[a]*

a. Department of Chemistry and Biochemistry, Montana State University, 103 Chemistry and Biochemistry Building, PO Box 173400, Bozeman MT 59717 United States

b. Centre for Enzyme Innovation, School of Biological Sciences, Institute of Biological and Biomedical Sciences, University of Portsmouth, PO1 2DY, United Kingdom

c. Renewable Resources and Enabling Sciences Center, National Renewable Energy Laboratory, Golden CO 80401 USA

d. Center for Bioenergy Innovation, Oak Ridge National Laboratory, Oak Ridge TN 37830 United States

* Corresponding authors ‡ Denotes equal contribution

Keywords: *biological funneling • cytochrome P450 • aromatic O-demethylation • protein engineering • lignin*

ABSTRACT: Biological funneling of lignin-derived aromatic compounds is a promising approach for valorizing its catalytic depolymerization products. Industrial processes for aromatic bioconversion will require efficient enzymes for key reactions, including demethylation of *O*-methoxy-aryl groups, an essential and often rate-limiting step. The recently characterized GcoAB cytochrome P450 system comprises a coupled monoxygenase (GcoA) and reductase (GcoB) that catalyzes oxidative demethylation of the *O*-methoxy-aryl group in guaiacol. Here, we evaluate a series of engineered GcoA variants for their ability to demethylate *o*-and *p*-vanillin, which are abundant lignin depolymerization products. Two rationally-designed, single amino acid substitutions, F169S and T296S, are required to convert GcoA into an efficient catalyst toward the *o*- and *p*-isomers of vanillin, respectively. Gain-of-function in each case is explained in light of an extensive series of enzyme-ligand structures, kinetic data, and molecular dynamics simulations. Using strains of *Pseudomonas putida* KT2440 already optimized for *p*-vanillin production from ferulate, we demonstrate demethylation by the T296S variant *in vivo*. This work expands the known aromatic *O*-demethylation capacity of cytochrome P450 enzymes towards important lignin-derived aromatic monomers.

Lignin is a primary structural polymer in plants that is derived from radical coupling reactions of *p*-coumaryl (H), coniferyl (G), and sinapyl (S) alcohols during cell wall biosynthesis.[1] In most plants, lignin is a heterogeneous structure linked by C-O and C-C bonds, which in turn leads to a heterogeneous slate of aromatic compounds upon catalytic or thermal depolymerization.[2-7] This inherent heterogeneity is the primary challenge in valorization of lignin to target chemicals. To overcome this challenge, the concept of biological funneling has been proposed.[5,8-16] Biological funneling harnesses microbial aromatic-catabolic pathways to convert diverse aromatic compounds into a minimal number of central intermediates.[8,17] The most common lignin funneling strategy relies on the production of aromatic *cis*-diols such as catechol or protocatechuate, which can undergo oxidative aromatic ring-cleavage reactions via dioxygenases. Aromatic *O*-demethylation is a critical reaction for biological funneling because G- and S-type alcohols, which exhibit 1 or 2 methoxyl groups adjacent to a phenolic hydroxyl group, respectively, are the most prevalent monolignols in most plants. Further, aromatic *O*-demethylation is a rate-limiting step in the production of bioproducts from G- and S-type aromatic compounds in engineered aromatic-catabolic strains.[18-19]

At least three enzyme classes – Rieske non-heme iron monooxygenases, tetrahydrofolate-dependent *O*-demethylases, and cytochrome P450 enzymes (hereafter P450s) – are known to catalyze aromatic *O*-demethylation.[20-26] P450s are powerful redox catalysts that have served as exceptionally useful scaffolds for biological transformations.[27] The P450 system at the heart of the current study was first identified by Eltis and colleagues, who demonstrated *O*-demethylation of guaiacol (2-methoxyphenol) (**Scheme 1A**), the simplest compound with a G-type substitution pattern on the aromatic ring, and reported the N-terminal sequence of the P450 oxygenase.[25,28] In 2018, Tumen-Velasquez, Johnson, and co-workers reported the full sequence, *in vivo* function, and an analysis of the evolution of the enzyme system (which was termed GcoAB) from *Amycolatopsis* sp.

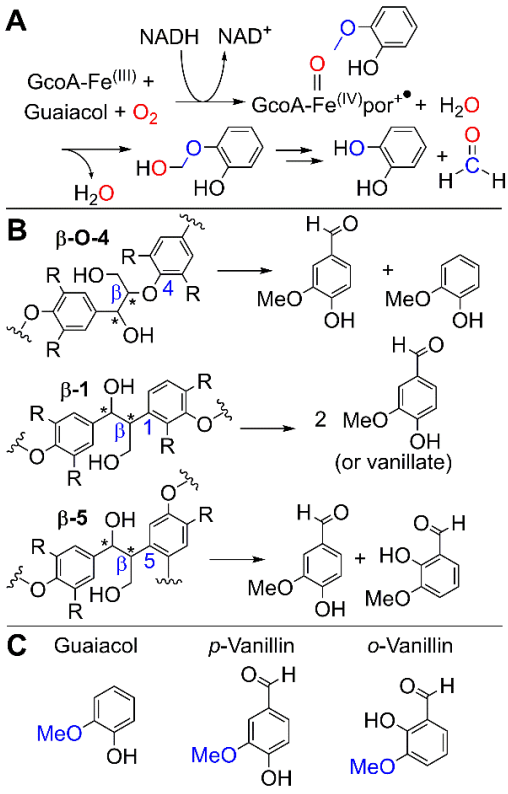

Scheme 1. (A) The chemical reaction natively catalyzed by the GcoAB enzyme system. The characteristic Compound I intermediate of P450s hydroxylates the substrate, forming an acetal which breaks down spontaneously to yield the formaldehyde and catechol products. (B) Common linkages between lignin subunits and *conceptual* chemical reactions that can yield *p*-vanillin (from β-O-4 and ring-opened β-1 bond cleavage) or *o*-vanillin (from β-5 bond cleavage). Chiral centers are indicated by asterisks. (C) Substrates used in this study.

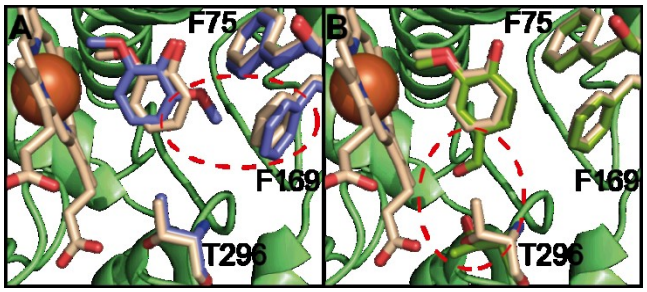

Figure 1. Structural comparisons of wild-type (WT) GcoA bound to the substrate guaiacol, syringol, and p-vanillin. (A) GcoA in complex with guaiacol (5NCB, tan) superimposed with GcoA-syringol (5OMU, blue). (B) GcoA-guaiacol (5NCB, tan), superimposed with GcoA-p-vanillin (5OMR, green). These structures provide a rationale for engineering.[25,28] Steric hindrance caused by the aromatic group of F169 or the secondary alcohol of T296 is highlighted with a red ellipse. Substitution with smaller hydrogen-bond donors may permit reactions with substrates bearing aldehyde groups in place of the methoxyl substituents indicated by the ellipses.

ATCC 39116.[24] This work was followed closely by Mallinson *et al*. with a detailed *in vitro* structural, biochemical, and computational characterization.[25] The GcoAB system represents a new architectural class of P450, with a cytochrome P450 monooxygenase (GcoA) and a three domain reductase (GcoB).[24-25] This system oxidatively demethylates guaiacol as its preferred substrate with excellent coupling of NADH oxidation to guaiacol turnover. It has been the subject of theoretical investigation[29] and has recently been successfully deployed in an engineered *E. coli* strain for the production of adipic acid.[30]

Most selective lignin depolymerization processes, however, yield products that exhibit additional ring functionality relative to guaiacol, with aromatic aldehydes being among the most abundant.[7] As shown in **Scheme 1B**, β-O-4 bond cleavage – by far the most well-studied reaction in lignin depolymerization chemistry[2-4,6-7] – can yield the *p*-vanillin aldehyde (4-hydroxy-3-methoxybenzaldehyde, commonly referred to simply as 'vanillin'). Cleavage of ring-opened β-1 C-C linkages or stilbene linkages can also yield two molar equivalents of *p*-vanillin.[31-34] β-5 linkages can conceptually yield one molar equivalent of *p*-vanillin and *o*-vanillin (2-hydroxy-3-methoxybenzaldehyde) (**Scheme 1B-C**).[35-36] The *Amycolatopsis* sp. ATCC 39116 GcoAB cytochrome P450 system (WP_020419855, WP_020419854) was therefore engineered for efficient turnover of aromatic aldehydes, specifically targeting *p*- and *o*-vanillin: substrates with which GcoAB has little to no native activity. Building from our previous work,[25,28] we employed structure-guided protein engineering in concert with detailed biochemical assays and molecular dynamics (MD) simulations to identify and characterize the appropriate GcoA active-site mutations (**Figure 1, S1**). To our delight, only single point mutations, unique to each substrate, were required to convert GcoAB into efficient biocatalysts for the turnover of these two vanillin isomers. Catabolism of *p*-vanillin was further demonstrated by heterologous expression of a variant enzyme in *Pseudomonas putida* KT2440, where the same variant was also able to efficiently demethylate the reduction product of *p*-vanillin (*p*-vanillyl alcohol). This work expands the known substrate specificity of P450s for lignin-relevant compounds and further demonstrates the potential applicability of this versatile demethylation system for biological funneling of lignin-derived aromatic compounds.

RESULTS

Single GcoA mutations at F169 or T296 yield *o*- and *p*-vanillin demethylation biocatalysts, respectively. Prior work on the GcoA-guaiacol co-structure (**Figure S1**) showed that F169 is a mobile active site residue that closely approaches the bound ligand (**Figure 1A**).[28] Substitution of F169 for a smaller hydrophobic counterpart (alanine) permits binding and demethylation of 2,6-dimethoxyphenol (syringol).[28] We hypothesized that this or another GcoA-F169 variant with a small side chain (such as valine or the hydrogen-bond donor, serine) might analogously accommodate an aldehyde group at the position *ortho* to the aryl hydroxyl (*o*-vanillin). These variants may therefore be capable of binding and demethylating *o*-vanillin, which is nearly isosteric with syringol. Examination of the WT GcoA structure with *p*-vanillin bound[25] (5NCB, 5OMR, respectively, **Figure 1B**) suggested an analogous strategy for engineering GcoA to bind and demethylate the *p*-vanillin isomer. Namely, the observed deflection in the T296 side chain toward the heme propionate in the *p*-vanillin versus the guaiacol complex indicated the need for a less sterically encumbered hydrogen bond donor at this position. We therefore examined the smaller hydrophobic (glycine, alanine) and hydrogen-bonding (serine) residues at this position (**Figure 1B**).

To address whether either *o*- or *p*-vanillin could serve as substrates of an engineered GcoA, we first quantified turnover of NADH in air within a fixed time (45 min) under different conditions (**Figure 2**, **Figure S3A**). In the presence of WT GcoAB but without an aromatic substrate, NADH consumption was not observed. This result is consistent with substrate-gating, a common feature of diverse P450 mechanisms[27] in which the oxidizable substrate/analog binds in the vicinity of the ferric heme and displaces a heme-bound water. This causes the spin state of iron to change from low (S=1/2) to high (S=5/2), priming it for one-electron reduction by NADH via the FAD-dependent reductase, GcoB. The reduced/ferrous heme iron then binds and reductively activates O_2, leading to oxygenation of the substrate.

The majority of NADH was consumed in the presence of WT GcoA and every GcoA amino acid monovariant (F169A/V/S, T296A/V/S) screened herein, regardless of which potential demethylation substrate (guaiacol, *o*-vanillin, or *p*-vanillin) was used. This suggests that the active site is sufficiently flexible to permit both aromatic substrate entry and water displacement in every case. However, significant (≥40%) coupling of NADH oxidation to vanillin demethylation was detected only for *o*-vanillin and the F169A/V/S variants, and separately, for *p*-vanillin/GcoA-T296S (**Figure 2**, **Table S1**). Notably, these variants gained the ability to demethylate their cognate aldehyde while maintaining substantial activity against the native GcoA substrate, guaiacol.

Reaction efficiency may be due to the ability of GcoA-F169A/V/S and -T296S to form productively-oriented complexes with *o*- and *p*-vanillin. To gain further information about the efficiency of the enzymes investigated here, we measured initial reaction rates (v_i), equilibrium dissociation constants (K_D), and apparent steady-state kinetic (k_{cat}, K_M) parameters for GcoA-F169S/*o*-vanillin and GcoA-T296S/*p*-vanillin in air (**Table S1**, **Figures S2-S5**). These variants were chosen for further

analysis, even though multiple F169 variants exhibited activity, since both

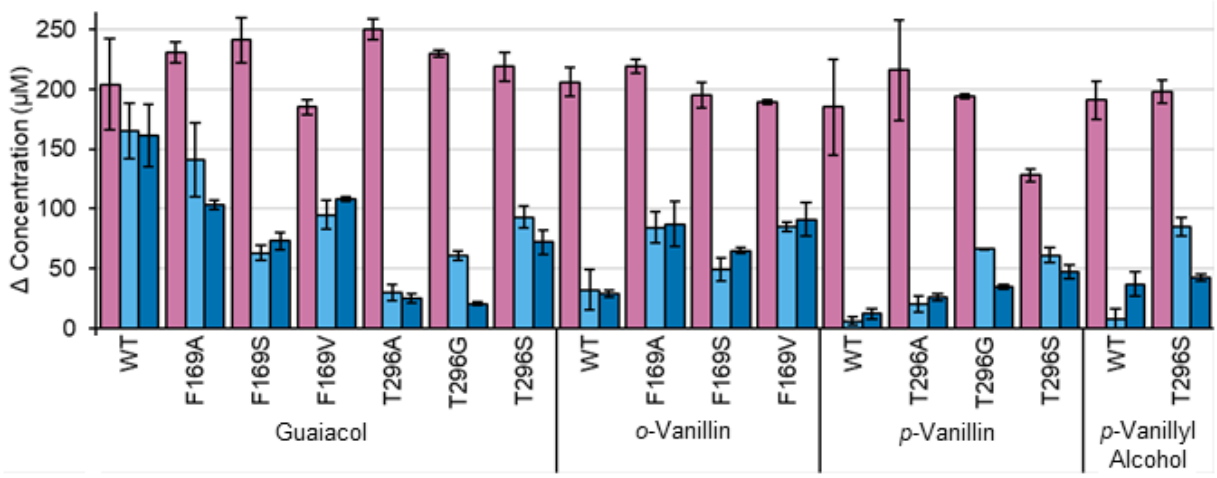

Figure 2. Coupling of substrate demethylation to NADH/O_2 consumption is illustrated by comparing the amounts of NADH (pink bars) and aromatic substrate consumed (light blue bars) or formaldehyde produced (dark blue bars) in an endpoint assay. Reaction mixtures contained equimolar GcoA and GcoB (0.2 – 0.5 μM), 100 μg/mL catalase, and 250 μM NADH in room temperature, air-saturated buffer (25 mM HEPES, 100 mM NaCl, pH 7.5, 210 μM O_2). Each reaction was initiated with a small volume (0.25-0.5 μL) of substrate stock (final concentrations: 250 μM guaiacol, *o*-vanillin, *p*-vanillyl alcohol; 100 μM *p*-vanillin). The consumption of NADH over time was monitored by UV/Vis absorption spectroscopy for 45 min. Reactions were quenched with concentrated H_2SO_4. Residual aromatic substrate concentrations were determined by HPLC, and formaldehyde concentrations were determined by a tryptophan-based colorimetric assay, as described in the Supporting Information.[37]

exhibited ≥40% coupling of NADH oxidation to vanillin demethylation after the introduction of the same primary alcohol (serine) near to the anticipated position of the aldehyde group of the substrate (**Figure 1**).

We hypothesized that efficient coupling would depend on multiple factors. First, a potential substrate must be able to enter the active site of GcoA, displace an iron-bound water, and bind above the porphyrin plane. To evaluate binding efficiency, values for K_D were measured by titrating the aromatic aldehydes into solutions of the ferric GcoA variants and directly observing formation of stable, equilibrium high spin enzyme-substrate complex via UV/vis spectroscopy (**Figure S2**). Though aldehyde binding to the WT GcoA was observable, the affinity of the enzyme for the native substrate (guaiacol) was 200- to 500-fold higher than for *o*- and *p*-vanillin, respectively (**Table S1**). The F169S and T296S variants like the WT exhibited an overall preference for binding guaiacol, the least sterically encumbered ligand, albeit with a 30-100-fold reduction in absolute affinity relative to the WT GcoA (**Table S1**). Each variant moreover exhibited a binding preference for the expected vanillin isomer (F169S/*o*-vanillin and T296S/*p*-vanillin) relative to the opposite isomer, with an affinity that was mostly unchanged relative to each vanillin/WT-GcoA pair. We concluded that GcoA-F169S and -T296S are capable of binding *o*- and *p*-vanillin, respectively, but that subsequent catalysis cannot be attributed to gains in vanillin equilibrium binding affinity by these variants.

We next evaluated how the set of aromatic substrates influenced the initial rates of NADH oxidation and aromatic product formation (saturating NADH, aromatic substrate, **Table S1**). NADH consumption is expected to be stimulated by substrate binding and water displacement from the heme, regardless of whether the substrate is demethylated. It was previously shown that the reducing equivalents spent in the uncoupled reaction could be quantitatively accounted for via the H_2O_2 produced, without significant uncatalyzed oxidation of the substrates or products under the reaction conditions used.[28] For WT GcoA, v_i(NADH consumption) was highest in the presence of excess guaiacol, followed closely by *o*-vanillin and *p*-vanillin (~3-fold decreases). The similarity in the magnitude of v_i(NADH) in the presence of all 3 aromatics, compared to the much larger differences in their equilibrium K_D values, suggests that v_i(NADH) largely reflects the aromatic on-rates (k_{on}) while K_D could be more strongly impacted by differences in their rates of departure (k_{off}, where $K_D = k_{on}/k_{off}$). Consistent with that interpretation, v_i(product formation) decreased by a far larger amount (20-30 fold) when the aldehydes were used, relative to the preferred substrate guaiacol. Collectively, these results suggest that the WT active site readily admits guaiacol and both vanillin isomers, but cannot retain or demethylate the latter.

By comparison, the F169S and T296S variants consumed NADH nearly as rapidly as WT GcoA in the presence of either guaiacol or their preferred vanillin isomers. However, strong deficits in v_i(NADH) were observed for F169S/*p*-vanillin and T296S/*o*-vanillin; similarly, v_i(product formation) for either F169S/*p*-vanillin or T296S/*o*-vanillin was effectively zero. Together, these results show that GcoA-F169S and -T296S GcoA exhibit strong selectivity for either guaiacol or their preferred vanillin isomers for *both* substrate entry and demethylation. These kinetic results are consistent with the high %-coupling of product formation to NADH consumption for F169S and T296S (**Figure 2**; for HPLC data illustrating product formation, see **Figure S4**).

Steady state kinetic parameters determined as a function of variable aromatic substrate (**Figure S5**) mirrored the trends in v_i and K_D. Namely, the turnover number (k_{cat}) remained high for WT/guaiacol and both variants, with the exception of F169S/*p*-

vanillin and T296S/*o*-vanillin. These combinations exhibited sharply impaired k_{cat}, in addition to v_i and K_D. The most telling patterns were observed in values measured for K_M (**Table S1**). In P450s, the Michaelis complex is presumed to contain Compound I, the ferryl-porphyrin cation radical that is poised to transfer an oxygen atom to the substrate. For WT GcoA, the values of K_M depended dramatically on the aromatic substrate choice, with K_M[*o*-vanillin] ≈ K_M[*p*-vanillin] >> K_M[guaiacol]. For F169S, K_M[*o*-vanillin] ≈ K_M[guaiacol], and the reaction with *p*-vanillin did not occur sufficiently to measure a value for K_M. Similarly, for T296S, K_M[*p*-vanillin] ≈ K_M[guaiacol]. No reaction was observed for *o*-vanillin. We could conclude that the F169S and T296S mutations therefore specifically stabilize the Michaelis complex with the cognate vanillin or the less encumbered substrate, guaiacol, thereby supporting catalysis.

Structural studies suggest a mechanism for substrate binding and turnover. To rationalize the observed biochemical results from a structural perspective, we employed a combination of X-ray crystallography and molecular dynamics simulations. The GcoA active site has been described as a tight-fitting hydrophobic pocket with a series of hydrophobic amino acids responsible for positioning the substrate's aromatic ring.[26] Binding of several different aromatic molecules with various ring substituents have shown accommodation with only subtle reorganization of the surrounding enzyme side chains, with varying results on turnover by GcoA.[26] Here, multiple crystal structures were successfully solved for engineered complexes of T296A/G/S:guaiacol (**Table S2**), T296A/G/S:*p*-vanillin (**Table S3**), and F169A/S/V:*o*-vanillin (**Table S4**). The resolution of these nine structures, ranging from 1.60-1.88 Å, allowed robust refinement of the bound ligand orientations and surrounding active site residue positions (**Figure S6**). Structures of T296A/G/S with the preferred substrate guaiacol revealed that this mutation was tolerated with minimal disruption to the active site (**Figure S7**). The structure of *o*-vanillin bound to GcoA-F169S indicates why this is a functionally productive complex, with the substrate aromatic ring adopting both the plane and relative rotation observed for guaiacol in the WT enzyme, thus providing the optimal presentation of the reactive methoxyl group towards the heme for catalysis. In parallel with the previously reported productive binding mode of syringol afforded by F169 mutations,[28] this larger cavity in the active site accommodates the aldehyde group of *o*-vanillin in an analogous mode to that previously observed with the additional methoxyl group of syringol (**Figure 3**, **Figure 1A**). The substrate orientation and ligand-heme distances are conserved between all three variants. The only significant difference with the WT is the relative rotation of residue F75, by 29° in F169V, 48° in F169A, and 53° in F169S (**Figure 3B**). Notably, all of these variants successfully demonstrated NADH oxidation coupled to demethylation of *o*-vanillin (**Figure 2**, **Table S1**).

While *o*-vanillin is isosteric with and parallels syringol binding, the *p*-isomer has an alternative set of spatial constraints that results in a steric clash with residue T296, generating an unproductive complex (5OMR, previously described, **Figure 1B**).[26] However, the T296S structure revealed that a small modification at this site not only created enough space to accommodate the aldehyde of *p*-vanillin unimpeded, but it also mitigates the shift observed in the heme propionate group closest to residue at 296 (**Figure 4A-B**). In the WT enzyme in complex with *p*-vanillin, the steric hindrance caused by the aldehyde group altered the propionate group orientation with a 35° torsional angle rotation moving the terminal oxygen by 1.5 Å, serving to disrupt the hydrogen bonding network with the arginine at position 298 and surrounding waters (**Figure 4A-C, S8**). Additionally, this shift caused a loss in a hydrogen bond between the arginine nitrogen and the propionate oxygen.

The co-crystal structures showed that all three residue 296 variants (A/G/S) positively affected the productive binding orientation of the *p*-vanillin substrate. The T296S variant was observed to be the most similar to that of the WT guaiacol complex, restoring both the water environment and the 3.0 Å distance between the R298 nitrogen and heme propionate oxygen (**Figure 4A, 4C, S8**), with the caveat that static crystallographic models offer rather limited insights towards such a dynamic system.

MD simulations were thus performed for 1) WT GcoA with guaiacol bound at the active site (PDB ID 5NCB), 2) WT GcoA with *p*-vanillin bound at the active site (PDB ID 5OMR), and 3) T296S with *p*-vanillin bound at the active site (**Figure S9**), revealing highly dynamic hydrogen bond patterns (**Figure 4D-F, S10**). The steric clash of the aldehyde group at the *ortho* position in *o*-vanillin with F169 is likely analogous to that of the syringol methoxy group studied in detail previously;[29] given the similarities in not only molecular structure but also structural and biochemical results *o*-vanillin was not examined here via MD. In each case, heme was modeled in the catalytically activated Compound I state, and 240 ns of dynamics were conducted.

The dual occupancy in the position of the S296 side chain observed in the crystal structure of GcoA-T296S bound with *p*-vanillin (**Figure 4C**) is observed to correlate with an alternating hydrogen bond with the nearer propionate and with the aldehyde group of the substrate (**Figure 4F**). A time trace of this behavior showed nearly twenty changes of S296 hydrogen bonding partners over the 240 ns simulation (**Figure S10**). As a result of this hydrogen bonding pattern, the crystal structure evidence indicated that the propionate positioning is restored to the position occupied in the WT GcoA bound with guaiacol (**Figure 4A**). The aldehyde orientation was also flipped from the orientation seen in the WT as a result of the T296S mutation both structurally (**Figure 4**, compare panels **B** and **C**) and computationally (**Figure 4**, compare panels **E** and **F**, though the aldehyde orientation was dynamic in the WT case; see **Figure S11**). Consistent with the crystal structure, simulations indicated that stable hydrogen bonding interactions between R298 and the propionate group in WT GcoA with guaiacol bound were disrupted when *p*-vanillin is bound and then dynamically restored when T296 is mutated to serine (**Figure S12**). The shift in distance was subtle (approximately 0.1-0.2 Å), but this is on par with the shift observed in structures (**Figure 4B**), wherein the hydrogen bonding interactions between R298 and propionate were weakened in the WT/vanillin case and restored in the T296S variant.

Comparison of the three simulations indicated that the ligand was significantly more mobile in the active site when *p*-vanillin is bound in WT GcoA, as compared to guaiacol (**Figure S11**). The T296S mutation facilitated stable positioning of *p*-vanillin in the same geometric range exhibited by guaiacol in WT GcoA (**Figure S11D**). The structure and dynamics of water molecules surrounding R298 also exhibited clear disruption in WT GcoA when *p*-vanillin was substituted for guaiacol (**Figure S13**). The restoration in the T296S variant, while not complete, was also

clear, especially in the first peak of the radial distribution function (RDF) but also in the second and third peaks. If it can be reasonably assumed that the mechanism of substrate accommodation for *o*-vanillin in the F169S variant is analogous to that of syringol in F169A (as argued above), the static and dynamic information revealed here by crystal structures and MD simulations, respectively, suggest the additional importance of restoring disrupted hydrogen bonding patterns at the active site for the accommodation of *p*-vanillin by GcoA T296S.

By analogy, the aldehyde group at the *ortho* position in *o*-vanillin is likely to have the same effect, given the similarities not only in molecular structure but also structural and biochemical results, and thus this was not studied further here. In contrast to the single site variants, crystallization of ligand-bound structures with substitutions at both sites (F169S/T296S) was largely unsuccessful, possibly indicating a reduction in either the stability or homogeneity of these enzyme preparations. One structure, of the F169A-T296S double variant complex with *p*-vanillin, was obtained, albeit at a lower resolution of 2.39 Å (**FiguresS6-S7**). Interestingly, *p*-vanillin also selectively stimulated NADH consumption by this variant (**Table S1**), suggesting that, in contrast to *o*-vanillin, this aldehyde was able to enter the active site and displace water. However, a stable equilibrium complex could not be observed via titrimetric methods, suggesting a high value for K_D (= k_{off} / k_{on}) potentially indicating an elevated k_{off}.

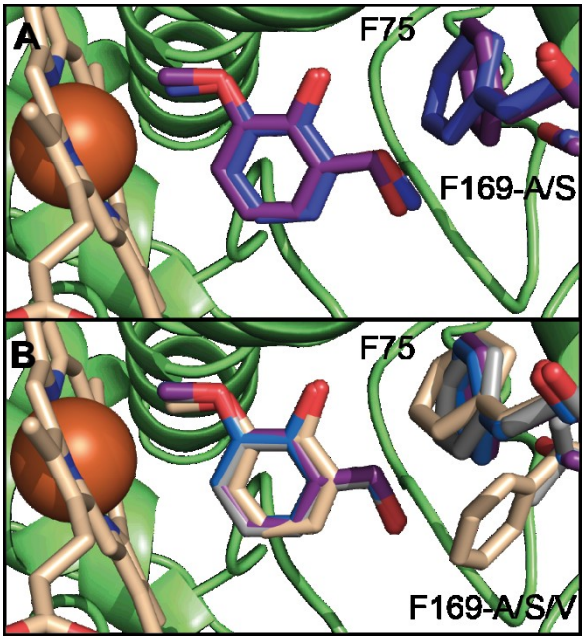

Figure 3. Binding mode of *o*-vanillin in comparison to guaiacol and syringol. **(A)** F169S in complex with *o*-vanillin (6YCO) superimposed with F169A-syringol (6HQQ). **(B)** F169A/S/V in complex with *o*-vanillin (6YCN, 6YCO, 6YCP) superimposed with WT GcoA-guaiacol (5NCB). The stepwise rotation of F75 is shown with the most divergent in the F169S variant, followed by F169A and F169V.

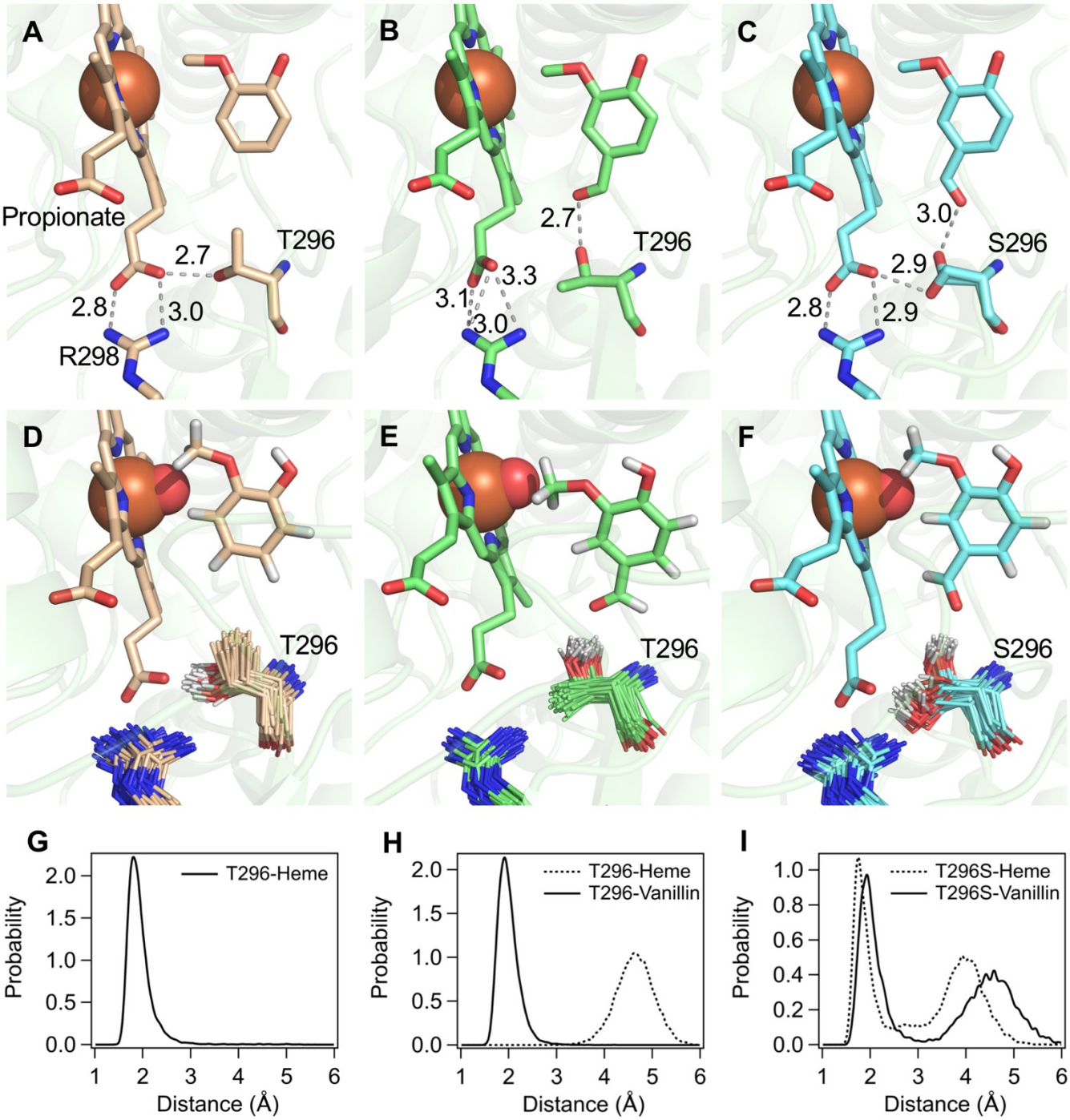

Figure 4. Binding mode of aromatic ligands in WT and variant GcoA in crystal structures and molecular simulations. (**A**) Crystal structure of guaiacol bound at the active site of WT GcoA (5NCB).[25] **(B)** WT GcoA structure in complex with *p*-vanillin (5OMR).[25] **(C)** GcoA T296S variant in complex with *p*-vanillin (6CYM). Also shown is the dual occupancy of the serine residue in position 296. Binding mode from MD for WT GcoA bound with guaiacol **(D)**, WT bound with *p*-vanillin (**E**), and T296S bound with *p*-vanillin (**F**). In D-F, the position of the sidechain of T296 or S296 (as well as R298) is shown every 2 ns over the course of a 240 ns MD simulation. The probability distributions of the hydrogen bond distance between T296 and the heme propionate group in WT/guaiacol system (**G**), between T296 and heme or vanillin in WT/vanillin system (**H**), and between S296 and heme or vanillin in T296S/vanillin system (**I**) reveal that T296 in WT stabilizes either heme when guaiacol is bound (A, D, G) or ligand when *p*-vanillin is bound (B, E, H), whereas the T296S residue stabilizes both heme and *p*-vanillin (C, F, I).

metabolite of ferulate metabolism in *P. putida*, by feruloyl-CoA synthetase (Fcs) and enoyl-CoA hydratase/aldolase (Ech) (**Figure 5A**).[39] In wild-type *P. putida* KT2440, *p*-vanillin is converted to vanillate and protocatechuate by vanillin dehydrogenase (Vdh) and vanillate *O*-demethylase (VanAB), respectively. However, deletion of the *vdh* gene and related aldehyde dehydrogenases, along with strong expression of *fcs-ech,* enables high *p*-vanillin yields from ferulate, as shown previously by Graf and Altenbuchner in *P. putida* strain GN442.[40] Here, we leveraged GN442 as a chassis to assess the efficacy of GcoA-

T296S as a *p*-vanillin demethylase *in vivo*. First, the *vanAB* gene was deleted from GN442 to produce strain ACB059, which precludes the "shunt" catabolic route through protocatechuate (**Figure 5**; SI methods; **Table S5**). Two variants were then constructed to express *gcoAB* under the strong P_{tac} promoter[41] in an ACB059 background: ACB086 expresses WT GcoA, while ACB087 expresses the variant GcoA-T296S (SI methods; **Table S5**). In both ACB086 and ACB087, *gcoA* was transcribed as a fusion with catechol 1,2-dioxygenase, *catAI*, as described previously,[24] because the chimeric protein (CatA, missing 4 C-terminal amino acids and linked to the full GcoA protein) catalyzes *O*-demethylation more rapidly than the individual proteins *in vivo*.

The three engineered strains and the KT2440 WT control were cultivated in shake flasks in minimal medium with 4 mM ferulate and 10 mM glucose to support growth (SI Methods). The growth rates of ACB059, ACB086, and ACB087 were nearly identical (**Figure S14**), but analysis of culture filtrates revealed distinct differences in the distribution of six key metabolites (**Figure 5B-D**). As expected, the KT2440 WT control consumed all ferulate within 13.5 h and none of the other five metabolites were detected (**Figure S15**). Conversely, the three engineered strains converted ferulate to a mixture of *p*-vanillin and vanillate (**Figure 5A**). Vanillate concentrations eventually plateaued, presumably as a result of the *vanAB* deletion, and protocatechuate was not detected in any sample. In all three engineered strains, the accumulated *p*-vanillin was depleted over time, and *p*-vanillin consumption was accompanied by production of vanillyl alcohol (vanillyl-OH; **Figure 5B-D**), likely due to activity of the recently described vanillin reductase, AreA (encoded by PP_2426).[42]

In ACB086 and ACB087, consumption of *p*-vanillin coincided with an increase in its demethylated product, protocatechuic aldehyde (PCAldehyde). Demethylated product yields in ACB086 remained relatively modest (0.04 mM PCAldehyde; maximum concentration), but ACB087 produced 0.10 mM PCAldehyde (maximum concentration) from 4 mM ferulate. The improved conversion of vanillin to PCAldehyde in strain ACB087 is in agreement with the *in vitro* observations, wherein the GcoA-T296S variant enzyme displayed substantially enhanced demethylation activity compared to native GcoA. Interestingly, concentrations of PCAldehyde decreased nearly to zero after 120 hours (**Figure S16**) while levels of 3,4-DHBA continued to increase, indicating reduction of PCAldehyde, perhaps by AreA.

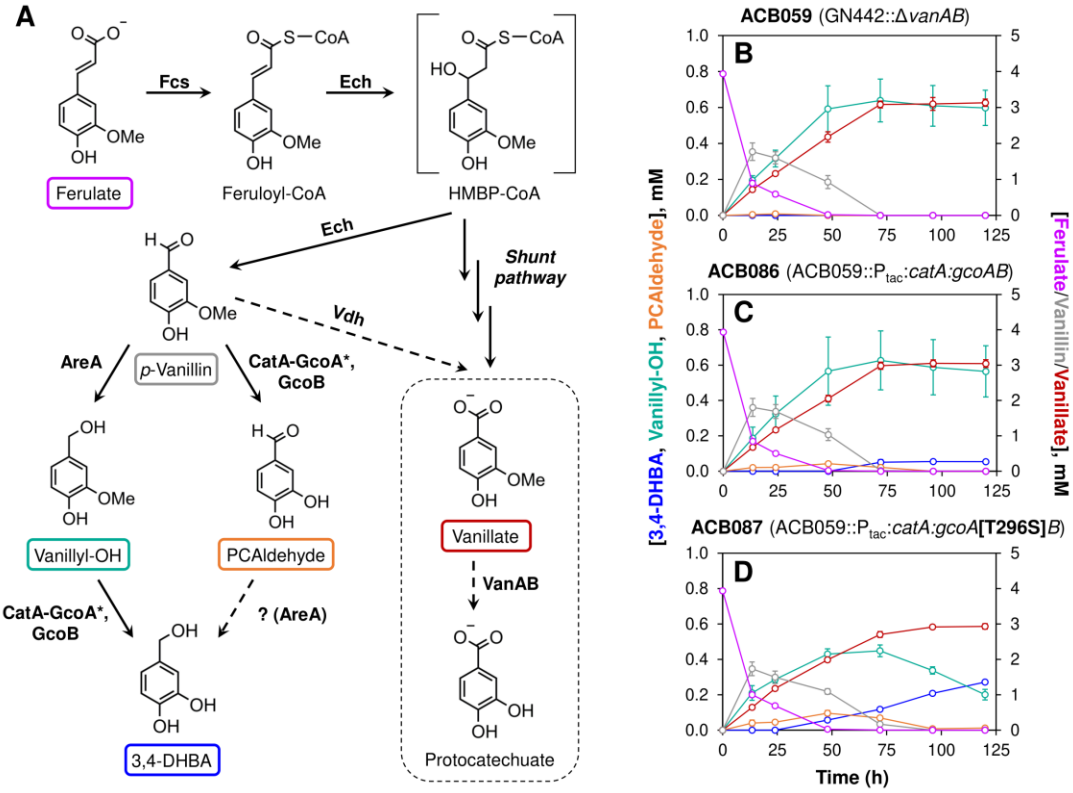

Figure 5. Expression of GcoA-T296S in *P. putida* KT2440 generates demethylated products from *p*-vanillin. **A)** Proposed route for the catabolism of ferulate in *P. putida* KT2440 WT and strains ACB059, ACB086, and ACB087. Compounds quantified by HPLC are indicated by the colored boxes, and the concentration of each compound in culture filtrates is plotted with respect to time for **(B)** ACB059, **(C)** ACB086, and **(D)** ACB087. In all three engineered strains, *vdh* and other aldehyde dehydrogenase genes (Table S5) were deleted to enhance accumulation of vanillin, and the *vanAB* genes were deleted to prevent formation of protocatechuate, which undergoes ring-opening for assimilation into central metabolism. The accumulated vanillin is converted to demethylated compounds, PCAldehyde and 3,4-DHBA, by GcoAB in ACB086 and GcoA[T296S]B in ACB087. The alternative "shunt" pathway, which routes HMBP-CoA through vanillyl-CoA to produce vanillate,[39] is also active in all three engineered strains. (Abbreviations: HMBP-CoA, 4-hydroxy-3-methoxyphenyl-β-ketopropionyl-CoA; Vanillyl-OH, vanillyl alcohol; PCAldehyde, protocatechuic aldehyde; 3,4-DHBA, 3,4-dihydroxybenzyl alcohol. *indicates GcoA is either WT or GcoA-T296S. Error bars indicate the standard deviation from the mean of three replicates.)

(**Figure 5A**). In both strains, particularly ACB087, accumulation of 3,4-DHBA was accompanied by consumption of vanillyl-OH, suggesting demethylase activity on both the aldehyde and alcohol forms of *p*-vanillin. Indeed, WT GcoA displayed 4 ± 4% coupling of vanillyl-OH demethylation to NADH/O_2 consumption *in vitro* while the GcoA-T296S variant displayed 43 ± 2% coupling (**Figure 2**), suggesting that the increased accumulation of 3,4-DHBA in strain ACB087 was in fact due to the superior activity of GcoA-T296S on both *p*-vanillin and vanillyl-OH. Additionally, in a separate experiment, strain ACB087 tolerated the addition of >1 mM exogenous H_2O_2 before exhibiting substantial growth defects (**Figure S17**), so it is unlikely that peroxides formed by uncoupling *in vivo* introduced an additional metabolic burden.

DISCUSSION

Biological funneling as a means of valorizing lignin will require the concerted action of multiple enzymes to reduce the complexity of deconstructed lignin streams to generate value-added products. This study describes two new cytochrome-P450 enzymes that catalyze the oxidative demethylation of *o*- and *p*-vanillin, which are aldehydes produced from the catalytic deconstruction of lignin. The resulting product catechol aldehydes can be further oxidized via central metabolic pathways common to many bacteria or harvested as valuable products. Notably, the new enzyme functions were generated via rational engineering based on high-resolution structures and the biocatalytic and dynamic properties of their natural precursor, GcoAB, a two-enzyme oxidoreductase system that specifically demethylates guaiacol and has only minimal demethylase activity toward the vanillins.[25,28]

Here, we observed that two single amino acid substitutions, each of which minimized steric clashes with and introduced hydrogen bond donors to the aldehyde groups, were sufficient to render GcoAB an effective catalyst towards the vanillin isomers. As expected, the *o*-vanillin binding mode with the F169S variant closely resembled that of the isosteric substrate syringol. This variant moreover efficiently catalyzed demethylation of *o*-vanillin as well as the less encumbered native substrate, guaiacol. Prior MD simulations suggested that the F169 sidechain is highly mobile and may be important for maintaining guaiaicol in its productive orientation.[25,28] Substitution of smaller residues at this position is required for ring-substituted guaiacol analogs, like syringol and *o*-vanillin, to stably achieve analogous productive binding modes.

Here, as with syringol,[25,28] we observed only small shifts in the crystallographic position of *p*-vanillin relative to the native substrate (guaiacol) bound to WT GcoA (**Figure 4A-C**); however, the *stability* of the ligand in that position in MD simulations is significantly affected. Substitution of the secondary alcohol (T296) for the primary (S296) was sufficient for restoring a WT-like hydrogen bonding pattern in the vicinity of the vanillin aldehyde group and, in turn, a dynamically stable binding mode that ultimately permits catalysis. The dynamic interaction between the substrate, heme propionate, R298, and a triad of crystallographically observed water molecules is apparently flexible enough to permit substitution of the sp^3-hybridized carbon of vanillyl alcohol, as this biological reduction product of *p*-vanillin was also efficiently demethylated by the T296S variant both *in vitro* (**Figure 2**, **Table S1**) and *in vivo* (**Figure 5**). Interestingly, catalysis by the engineered enzyme variants is not due to enhancements in the efficiency of water displacement from the active site by the aldehydes (represented by v_i(NADH)), nor to increases in equilibrium binding affinity (K_D) (**Table S1**). Rather, catalysis correlates with a lowering of K_M for the successful enzyme variant/substrate pairs, indicating an increased probability of forming the productive enzyme-substrate near-attack conformation. Structurally, this corresponds to precise orientation of the reactive methoxyl group and the adjoining aromatic ring into a productive configuration defined by the binding mode for the native substrate, guaiacol. Computationally, we see that retention of the demethylation substrate in the near attack conformation is likely mediated by hydrophobic interactions in the case of *o*-vanillin, and by a network of second-sphere hydrogen bonds linking the substrate and heme to the protein environment for *p*-vanillin and its cognate alcohol.

CONCLUSIONS

We have demonstrated that GcoAB and its single amino acid variants can catalyze a wide range of aromatic *O*-demethylations that previously constituted critical bottlenecks to biological funneling of lignin. These novel catalysts are robust both *in vitro* and in synthetic biology/*in vivo* systems, bringing this longstanding holy grail of renewable carbon capture ever closer to actualization. This work further highlights the extraordinary catalytic flexibility of bacterial cytochrome P450 systems, their amenability to structure-guided engineering approaches, and their particular applicability to the lignin funneling problem. Our efforts have resulted in a set of P450s, interacting with a common reductase (GcoB) that now permit demethylation of all of the canonical aromatic lignin subunits. Acquisition of the full set of catalytic functions required for lignin funneling, through a combination of enzyme discovery and engineering, serves as the necessary starting point from which directed evolution and practical synthetic strain development can follow.

EXPERIMENTAL METHODS

Protein Expression and Purification. Mutagenesis was performed using primers listed in SI Appendix, with the Q5 polymerase and KLD enzyme mix (New England BioLabs) according to the manufacturer's protocol. Proteins were expressed as described previously.

Ligand Binding and Activity Assays. Enzyme/ligand dissociation constants were measured via changes in the UV/vis spectrum of the GcoA-bound heme. Enzyme activity was monitored continuously via the UV/vis absorbance of NADH, and discontinuously by HPLC, as described previously.

Crystallization and Structure Determination. Crystallization, diffraction experiments, and structure solution were carried out as described previously.

Molecular Dynamics Simulations. MD simulations were performed with an approach similar to our previous work.[25,28] Models were constructed from ligand bound crystal structures of GcoA and simulated using the Generalized Amber Force Field (GAFF)[43] in the NAMD molecular simulation program[44]. Further details can be found in the Supporting Information.

Strain construction, cultivation, and metabolite analysis. A detailed description of the construction and cultivation of *P. putida* strains ACB059, ACB086, and ACB087 is provided in the SI Appendix and Tables S4-S6, along with analytical methods for metabolite quantification by HPLC.

Data Deposition. The atomic coordinates and structure factors have been deposited in the Protein Data Bank, https://www.wwpdb.org (PDB ID codes 6CYH, 6CYI, 6CYJ, 6CYK, 6CYL, 6CYM, 6CYN, 6CYO, 6CYP, 6CYT).

ASSOCIATED CONTENT

Supporting Information includes: Detailed experimental methods; Figures S1-S13; Tables S1-S7.This material is available free of charge via the Internet at http://pubs.acs.org

AUTHOR INFORMATION

Corresponding Author

* jennifer.dubois1@montana.edu, john.mcgeehan@port.ac.uk, and gregg.beckham@nrel.gov

Present Addresses

† Current Address: Biosciences Center, National Renewable Energy Laboratory, 15013 Denver West Parkway, Golden CO 80401 United States

¶ Current Address: Department of Chemistry, University of Illinois Urbana-Champaign, 600 South Mathews Avenue, Urbana, IL 61801 United States

Author Contributions

The manuscript was written through contributions of all authors. / All authors have given approval to the final version of the manuscript.

‡These authors contributed equally.

Funding Sources

This work was partially authored by Alliance for Sustainable Energy, LLC, the manager and operator of NREL for the U.S. Department of Energy (DOE) under Contract No. DE-AC36-08GO28308. AB, DJH, JEM, and GTB acknowledge funding from The Center for Bioenergy Innovation, which is a U.S. DOE Bioenergy Research Center supported by the Office of Biological and Environmental Research in the DOE Office of Science. LB, CWJ, BCK, and GTB acknowledge funding from the U.S. DOE Office of Energy Efficiency and Renewable Energy Bioenergy Technologies Office. ESE, MMM, BRS, QVD, and JLD obtained financial support for this work from the US National Science Foundation grant MCB1715176. JEM acknowledges Research England for E3 funding and the BBSRC for grant BB/P011918/1 and a studentship to SJBM. The Diamond Light Source provided access and support to beamlines I03 and I04 under proposals MX17212 and MX23269. Computer time was provided by the National Renewable Energy Laboratory Computational Sciences Center supported by the DOE Office of EERE under contract number DE-AC36-08GO28308. The views expressed in the article do not necessarily represent the views of the DOE or the U.S. Government. The U.S. Government retains and the publisher, by accepting the article for publication, acknowledges that the U.S. Government retains a nonexclusive, paid-up, irrevocable, worldwide license to publish or reproduce the published form of this work, or allow others to do so, for U.S. Government purposes.

ACKNOWLEDGMENT

We thank Josef Altenbuchner of Universität Stuttgart for the generous gift of *P. putida* GN442 and Eugene Kuatsjah of the National Renewable Energy Laboratory for critical reading of the manuscript.

ABBREVIATIONS

P450, cytochrome P450; WT, wild type; FAD, flavin adenine dinucleotide; NADH, nicotinamide adenine dinucleotide; v_i, initial rate; MD, molecular dynamics; RDF, radial distribution function; Fcs, feruloyl-CoA synthetase; Ech, enoyl-CoA hydratase/aldolase; HMBP-CoA, 4-hydroxy-3-methoxyphenyl-β-ketopropionyl-CoA; Vanillyl-OH, vanillyl alcohol; PCAldehyde, protocatechuic aldehyde; 3,4-DHBA, 3,4-dihydroxybenzyl alcohol.

REFERENCES

(1) Vanholme, R.; Demedts, B.; Morreel, K.; Ralph, J.; Boerjan, W., Lignin Biosynthesis and Structure. *Plant Physiology* **2010,** *153* (3), 895-905.

(2) Zakzeski, J.; Bruijnincx, P. C.; Jongerius, A. L.; Weckhuysen, B. M., The Catalytic Valorization of Lignin for the Production of Renewable Chemicals. *Chem. Rev.* **2010,** *110* (6), 3552-3599.

(3) Ragauskas, A. J.; Beckham, G. T.; Biddy, M. J.; Chandra, R.; Chen, F.; Davis, M. F.; Davison, B. H.; Dixon, R. A.; Gilna, P.; Keller, M., Lignin Valorization: Improving Lignin Processing in the Biorefinery. *Science* **2014,** *344* (6185), 709-718.

(4) Rinaldi, R.; Jastrzebski, R.; Clough, M. T.; Ralph, J.; Kennema, M.; Bruijnincx, P. C.; Weckhuysen, B. M., Paving the Way for Lignin Valorisation: Recent Advances in Bioengineering, Biorefining and Catalysis. *Angew. Chem. Int. Ed.* **2016,** *55* (29), 8164-8215.

(5) Beckham, G. T.; Johnson, C. W.; Karp, E. M.; Salvachúa, D.; Vardon, D. R., Opportunities and Challenges in Biological Lignin Valorization. *Curr. Opin. Biotech.* **2016,** *42*, 40-53.

(6) Sun, Z.; Fridrich, B. l.; de Santi, A.; Elangovan, S.; Barta, K., Bright Side of Lignin Depolymerization: Toward New Platform Chemicals. *Chem. Rev.* **2018,** *118* (2), 614-678.

(7) Schutyser, W.; Renders, a. T.; Van den Bosch, S.; Koelewijn, S.-F.; Beckham, G.; Sels, B. F., Chemicals from Lignin: An Interplay of Lignocellulose Fractionation, Depolymerisation, and Upgrading. *Chem. Soc. Rev.* **2018,** *47* (3), 852-908.

(8) Linger, J. G.; Vardon, D. R.; Guarnieri, M. T.; Karp, E. M.; Hunsinger, G. B.; Franden, M. A.; Johnson, C. W.; Chupka, G.; Strathmann, T. J.; Pienkos, P. T., Lignin Valorization through Integrated Biological Funneling and Chemical Catalysis. *Proc. Natl. Acad. Sci.* **2014,** *111* (33), 12013-12018.

(9) Salvachúa, D.; Karp, E. M.; Nimlos, C. T.; Vardon, D. R.; Beckham, G. T., Towards Lignin Consolidated Bioprocessing: Simultaneous Lignin Depolymerization and Product Generation by Bacteria. *Green Chem.* **2015,** *17* (11), 4951-4967.

(10) Vardon, D. R.; Franden, M. A.; Johnson, C. W.; Karp, E. M.; Guarnieri, M. T.; Linger, J. G.; Salm, M. J.; Strathmann, T. J.; Beckham, G. T., Adipic Acid Production from Lignin. *Energy Environ. Sci.* **2015,** *8* (2), 617-628.

(11) Kamimura, N.; Takahashi, K.; Mori, K.; Araki, T.; Fujita, M.; Higuchi, Y.; Masai, E., Bacterial Catabolism of Lignin-Derived Aromatics: New Findings in a Recent Decade: Update on Bacterial Lignin Catabolism. *Environ. Microbiol. Rep.* **2017,** *9* (6), 679-705.

(12) Eltis, L. D.; Singh, R., Biological Funneling as a Means of Transforming Lignin-Derived Aromatic Compounds into Value-Added Chemicals. In *Lignin Valorization: Emerging Approaches*, Beckham, G. T., Ed. Royal Society of Chemistry: 2018; pp 290-313.

(13) Liu, Z.-H.; Yuan, J. S., Systems Biology Analyses of Lignin Conversion. In *Lignin Valorization: Emerging Approaches*, Beckham, G. T., Ed. Royal Society of Chemistry: 2018; pp 314-332.

(14) Seaton, S. C.; Neidle, E. L., Using Aerobic Pathways for Aromatic Compound Degradation to Engineer Lignin Metabolism. In *Lignin Valorization: Emerging Approaches*, Beckham, G. T., Ed. Royal Society of Chemistry: 2018; pp 252-289.
(15) Becker, J.; Wittmann, C., A Field of Dreams: Lignin Valorization into Chemicals, Materials, Fuels, and Health-Care Products. *Biotechnol. Adv.* **2019,** *37* (6), 107360-107384.
(16) Bugg, T. D.; Williamson, J. J.; Rashid, G. M., Bacterial Enzymes for Lignin Depolymerisation: New Biocatalysts for Generation of Renewable Chemicals from Biomass. *Curr. Opin. Chem. Biol.* **2020,** *55*, 26-33.
(17) Fuchs, G.; Boll, M.; Heider, J., Microbial Degradation of Aromatic Compounds - from One Strategy to Four. *Nat. Rev. Microbiol.* **2011,** *9* (11), 803-816.
(18) Johnson, C. W.; Abraham, P. E.; Linger, J. G.; Khanna, P.; Hettich, R. L.; Beckham, G. T., Eliminating a Global Regulator of Carbon Catabolite Repression Enhances the Conversion of Aromatic Lignin Monomers to Muconate in Pseudomonas Putida Kt2440. *Metab. Eng. Commun.* **2017,** *5*, 19-25.
(19) Salvachúa, D.; Johnson, C. W.; Singer, C. A.; Rohrer, H.; Peterson, D. J.; Black, B. A.; Knapp, A.; Beckham, G. T., Bioprocess Development for Muconic Acid Production from Aromatic Compounds and Lignin. *Green Chem.* **2018,** *20* (21), 5007-5019.
(20) Sutherland, J. B., Demethylation of Veratrole by Cytochrome P-450 in Streptomyces Setonii. *Appl. Environ. Microbiol.* **1986,** *52* (1), 98-100.
(21) Eltis, L. D.; Karlson, U.; Timmis, K. N., Purification and Characterization of Cytochrome P450rr1 from Rhodococcus Rhodochrous. *Eur. J. Biochem.* **1993,** *213* (1), 211-216.
(22) Karlson, U.; Dwyer, D.; Hooper, S.; Moore, E.; Timmis, K.; Eltis, L., Two Independently Regulated Cytochromes P-450 in a Rhodococcus Rhodochrous Strain That Degrades 2-Ethoxyphenol and 4-Methoxybenzoate. *J. Bacteriology* **1993,** *175* (5), 1467-1474.
(23) Kawahara, N.; Ikatsu, H.; Kawata, H.; Miyoshi, S.-i.; Tomochika, K.-i.; Sinoda, S., Purification and Characterization of 2-Ethoxyphenol-Induced Cytochrome P450 from Corynebacterium Sp. Strain Ep1. *Can. J. Microbiol.* **1999,** *45* (10), 833-839.
(24) Tumen-Velasquez, M.; Johnson, C. W.; Ahmed, A.; Dominick, G.; Fulk, E. M.; Khanna, P.; Lee, S. A.; Schmidt, A. L.; Linger, J. G.; Eiteman, M. A., Accelerating Pathway Evolution by Increasing the Gene Dosage of Chromosomal Segments. *Proc. Natl. Acad. Sci.* **2018,** *115* (27), 7105-7110.
(25) Mallinson, S. J.; Machovina, M. M.; Silveira, R. L.; Garcia-Borràs, M.; Gallup, N.; Johnson, C. W.; Allen, M. D.; Skaf, M. S.; Crowley, M. F.; Neidle, E. L., A Promiscuous Cytochrome P450 Aromatic O-Demethylase for Lignin Bioconversion. *Nat. Commun.* **2018,** *9* (1), 1-12.
(26) Fetherolf, M. M.; Levy-Booth, D. J.; Navas, L. E.; Liu, J.; Grigg, J. C.; Wilson, A.; Katahira, R.; Beckham, G. T.; Mohn, W. W.; Eltis, L. D., Characterization of Alkylguaiacol-Degrading Cytochromes P450 for the Biocatalytic Valorization of Lignin. *Proc. Natl. Acad. Sci.* **2020,** *117* (41), 25771-25778.
(27) Li, Z.; Jiang, Y.; Guengerich, F. P.; Ma, L.; Li, S.; Zhang, W., Engineering Cytochrome P450 Enzyme Systems for Biomedical and Biotechnological Applications. *J. Biol. Chem.* **2020,** *295* (3), 833-849.
(28) Machovina, M. M.; Mallinson, S. J.; Knott, B. C.; Meyers, A. W.; Garcia-Borràs, M.; Bu, L.; Gado, J. E.; Oliver, A.; Schmidt, G. P.; Hinchen, D. J., Enabling Microbial Syringol Conversion through Structure-Guided Protein Engineering. *Proc. Natl. Acad. Sci.* **2019,** *116* (28), 13970-13976.
(29) Ali, H. S.; Henchman, R.; de Visser, S., Lignin Biodegradation by a Cytochrome P450 Enzyme: A Computational Study into Syringol Activation by Gcoa. *Eur. J. Chem.* **2020,** *26* (57), 13093-13102.
(30) Suitor, J. T.; Varzandeh, S.; Wallace, S., One-Pot Synthesis of Adipic Acid from Guaiacol in Escherichia Coli. *ACS Synth. Biol.* **2020,** *9* (9), 2472-2476.
(31) Sedai, B.; Diaz-Urrutia, C.; Baker, R. T.; Wu, R.; Silks, L. P.; Hanson, S. K., Aerobic Oxidation of B-1 Lignin Model Compounds with Copper and Oxovanadium Catalysts. *ACS Catalysis* **2013,** *3* (12), 3111-3122.
(32) Liu, H.; Li, H.; Luo, N.; Wang, F., Visible-Light-Induced Oxidative Lignin C–C Bond Cleavage to Aldehydes Using Vanadium Catalysts. *ACS Catalysis* **2019,** *10* (1), 632-643.
(33) Kuatsjah, E.; Verstraete, M. M.; Kobylarz, M. J.; Liu, A. K.; Murphy, M. E.; Eltis, L. D., Identification of Functionally Important Residues and Structural Features in a Bacterial Lignostilbene Dioxygenase. *J. Biol. Chem.* **2019,** *294* (35), 12911-12920.
(34) Presley, G. N.; Werner, A. Z.; Katahira, R.; Garcia, D. C.; Haugen, S. J.; Ramirez, K. J.; Giannone, R. J.; Beckham, G. T.; Michener, J. K., Pathway Discovery and Engineering for Cleavage of a ß-1 Lignin-Derived Biaryl Compound. *Metab. Eng.* **In review,** *117* (41), 25771-25778.
(35) Katahira, R.; Elder, T. J., A Brief Introduction to Lignin Structure. In *Lignin Valorization: Emerging Approaches*, Beckham, G. T., Ed. Royal Society of Chemistry: 2018; pp 1-20.
(36) Takahashi, K.; Kamimura, N.; Hishiyama, S.; Hara, H.; Kasai, D.; Katayama, Y.; Fukuda, M.; Kajita, S.; Masai, E., Characterization of the Catabolic Pathway for a Phenylcoumaran-Type Lignin-Derived Biaryl in Sphingobium Sp. Strain Syk-6. *Biodegradation* **2014,** *25* (5), 735-745.
(37) Chrastil, J.; Wilson, J. T., A Sensitive Colorimetric Method for Formaldehyde. *Anal. Biochem.* **1974,** *63* (1), 202-207.
(38) Nikel, P. I.; Martínez-García, E.; de Lorenzo, V., Biotechnological Domestication of Pseudomonads Using Synthetic Biology. *Nat. Rev. Microbiol.* **2014,** *12* (5), 368-379.
(39) Graf, N.; Altenbuchner, J., Genetic Engineering of Pseudomonas Putida Kt2440 for Rapid and High-Yield Production of Vanillin from Ferulic Acid. *Appl. Microbiol. Biotech.* **2014,** *98* (1), 137-149.
(40) Plaggenborg, R.; Overhage, J.; Steinbüchel, A.; Priefert, H., Functional Analyses of Genes Involved in the Metabolism of Ferulic Acid in Pseudomonas Putida Kt2440. *Appl. Microbiol. Biotech.* **2003,** *61* (5-6), 528-535.
(41) De Boer, H. A.; Comstock, L. J.; Vasser, M., The Tac Promoter: A Functional Hybrid Derived from the Trp and Lac Promoters. *Proc. Natl. Acad. Sci.* **1983,** *80* (1), 21-25.
(42) García-Hidalgo, J.; Brink, D. P.; Ravi, K.; Paul, C. J.; Lidén, G.; Gorwa-Grauslund, M. F., Vanillin Production in Pseudomonas: Whole-Genome Sequencing of Pseudomonas Sp. Strain 9.1 and Reannotation of Pseudomonas Putida Cala as a Vanillin Reductase. *Appl. Environ. Microbiol.* **2020,** *86* (6), 1-17.
(43) Wang, J.; Wang, W.; Kollman, P. A.; Case, D. A., Automatic Atom Type and Bond Type Perception in Molecular Mechanical Calculations. *J. Mol. Graph. Model.* **2006,** *25* (2), 247-260.
(44) Phillips, J. C.; Braun, R.; Wang, W.; Gumbart, J.; Tajkhorshid, E.; Villa, E.; Chipot, C.; Skeel, R. D.; Kale, L.; Schulten, K., Scalable Molecular Dynamics with Namd. *J. Comput. Chem.* **2005,** *26* (16), 1781-1802.

For Table of Contents Only: